

Chemical characteristics and composition of hydrothermal biotite from the Dalli porphyry copper prospect, Arak, central province of Iran

F. Ayati · F. Yavuz · M. Noghreyan · H. A. Haroni ·
R. Yavuz

Received: 6 November 2007 / Accepted: 4 March 2008 / Published online: 7 May 2008
© Springer-Verlag 2008

Abstract The Dalli porphyry copper deposit is hosted by the Miocene–Pliocene subvolcanic plutons with chemical composition from diorite to granodiorite that intruded into the andesitic and dacitic volcanic rocks and variety of sedimentary sequences within the Urumieh–Dokhtar Magmatic Arc. Three main hydrothermal alteration zones including potassic, phyllic and propylitic types have been described in the volcano-plutonic rocks. Early hydrothermal alteration started with potassic style in the central part of system produced a secondary biotite–K-feldspar–magnetite assemblage and accompanies to chalcopyrite and pyrite

mineralization. This paper summarizes the detailed biotite mineral chemistry from the potassic and phyllic alteration zones. The FeO, TiO₂, MnO, K₂O, and Na₂O (wt.%) concentrations of biotite from the phyllic alteration zone are lower than biotite from the potassic alteration zone. The F and Cl (wt.%) contents of biotite from the potassic alteration zone display relatively high positive correlation with the X_{Mg} . The fluorine intercept values [IV (F)] from the potassic and phyllic alteration zones are strongly positively correlated with the fluorine/chlorine intercept values [IV (F/Cl)]. Biotite geothermometry for the potassic and phyllic alteration zones yield a range from 402° to 450°C and 280° to 343°C, respectively at Dalli porphyry copper deposit. The scatter in log (X_F/X_{OH}) ratios vs. X_{Mg} and X_{Fe} plots also reflects the evidence of biotite formed under dissimilar composition and temperature conditions in the potassic and phyllic alteration zones. Calculated log fugacity ratios of (f_{H_2O}/f_{HF}), (f_{H_2O}/f_{HCl}), and (f_{HF}/f_{HCl}) show that hydrothermal fluids associated with the potassic alteration were distinctively different from fluids those associated with the phyllic alteration zone at Dalli porphyry copper deposit. The relation between log (f_{H_2O}/f_{HCl}) and log (f_{H_2O}/f_{HF}) fugacity ratios indicates that biotite from the Dalli volcano-plutonic rocks is distinctly similar to biotite from the porphyry copper deposit at Bingham.

Editorial handling: A. Beran

F. Ayati · M. Noghreyan
Department of Geology, Isfahan University,
Isfahan, Iran

F. Ayati
e-mail: F_ayati@geol.ui.ac.ir

M. Noghreyan
e-mail: noghreyan.moussa@sci.ui.ac.ir

F. Yavuz (✉)
Jeoloji Mühendisliği Bölümü,
İstanbul Teknik Üniversitesi,
Maslak, İstanbul, Turkey
e-mail: yavuz@itu.edu.tr

H. A. Haroni
Department of Mining,
Isfahan University of Technology,
Isfahan, Iran
e-mail: hooshang@cc.iut.ac.ir

R. Yavuz
Kimya Mühendisliği Bölümü,
İstanbul Teknik Üniversitesi,
Maslak, İstanbul, Turkey
e-mail: kmyavuz@itu.edu.tr

Introduction

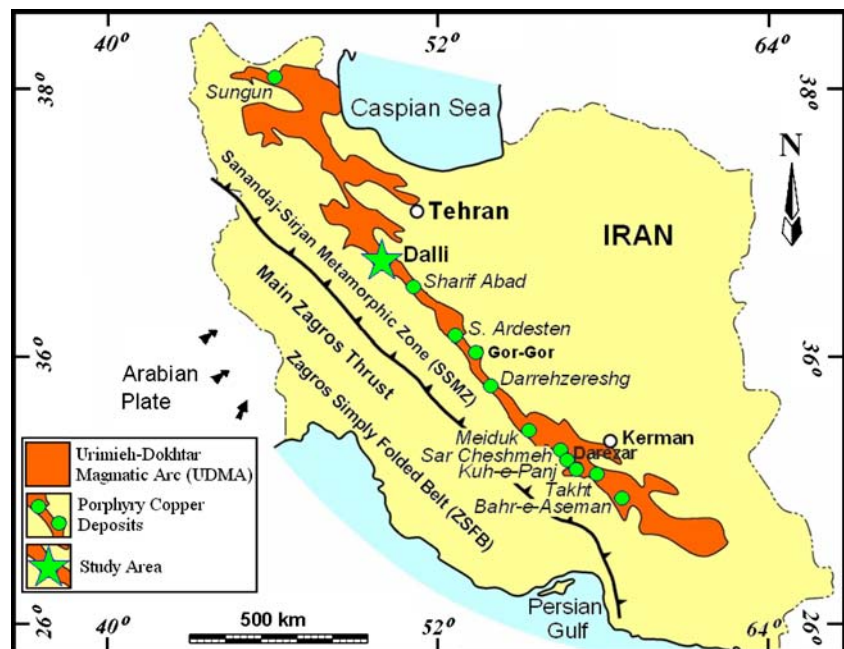
In the 10,000 km-long Alpine–Himalayan orogenic and metallogenic belt, there have been discovered numerous porphyry copper deposits such as Recks-Lahóca in Hungary (Gatter et al. 1999), Rosia Poeni in Romania (Milu et al. 2004), Veliki Krivelj in former Yugoslavia (Jelanković and

Vakanjac 1999), Assarel in Bulgaria (Angelkov and Parvanov 1980), Maronia in Greece (Melfos et al. 2002), Güzelyayla in Turkey (Yavuz 1997), Sungun, Raigan, and Sar-Cheshmeh in Iran (Hezarkhani and Williams-Jones 1998; Hezarkhani 2006a, b), and Saindak in Pakistan (Sillitoe and Khan 1977). The calc-alkaline volcano-plutonic rocks of Urumieh–Dokhtar Magmatic Arc (UDMA) host several porphyry type deposits, and in some places disseminated and vein-type base metal and precious metal deposits. In the UDMA, the Sungun and Sar-Cheshmeh porphyry copper deposits are presently mined for Cu and Mo, but this belt still has a great potential for undiscovered porphyry style $\text{Cu}\pm\text{Mo}\pm\text{Au}$ deposits. The most important and large porphyry deposits in Iran, currently mined and active mines, are located in the NW and SE of the UDMA. The Sar-Cheshmeh porphyry system (~1,200 Mt at 0.64% Cu, 0.03% Mo and 0.02 g/t Au) and the Sungun porphyry system (~900 Mt at 0.76% Cu and 0.06% Mo) are located in the SE and NW location of the UDMA, respectively. Ore deposits associated with the porphyry system of UDMA are generally accompanied to Miocene granitoids with dominant rock composition from granodiorite to quartz–monzonite stocks. In this magmatic arc, porphyry-type mineralization is typically found within the potassic and phyllic alteration zones.

Although the majority of well-known porphyry copper deposits in Iran have been studied in terms of base metal contents, fluid inclusion characteristics, stable isotopes, and alteration geochemistry (Hezarkhani and Williams-Jones 1998; Zarasvandi et al. 2005; Hezarkhani 2006a, b), there have been no investigation focusing on the biotite halogen chemistry and hydrothermal fluid fugacity ratios that play

an important role in determining the physicochemical conditions of alteration and mineralization processes in porphyry-type deposits. The aim of this study is mainly guided to the biotite chemistry from the newly discovered Au-rich Dalli porphyry copper deposit that was formed during a major period of hydrothermal alteration associated with the emplacement of Miocene–Pliocene volcano-plutonic rocks in the central province of Iran. The Dalli porphyry copper deposit accompanies to calc-alkaline porphyritic volcano-plutonic rocks (VPR) in the UDMA, which is characterized by the presence of widespread Neo-Tethys magmatism and mineralization in central Iran. The Dalli porphyry system with an average grade of 1.2 ppm Au and 0.75% Cu is the only reported Cu–Au porphyry deposit located in the western margin of the central UDMA with the NW–SE trending structures (Fig. 1). Three mineralized porphyry centers at Dalli crop out within a NE–SW trending corridor of altered Neogene intrusives with rock composition from porphyry diorite to tonalite that intruded into the volcanic rocks, which are dominantly in andesitic and dacitic composition, and pyroclastics in Miocene age. The mineralized intrusives at Dalli are affected by intensive potassic alteration (secondary biotite–K-feldspar–magnetite–quartz assemblage with strong stockworks and ore veins) with overprinting phyllic alteration (quartz–sericite–chlorite–specularite assemblage) and strong silicification processes. Potassic and phyllic alteration assemblages are surrounded by an extensive propylitic alteration zone at a distance from the porphyry stock. The whole alteration system covers roughly an area of 3×6.5 km in the Dalli area (Fig. 2). In this study, we document the occurrence of hydrothermal biotites from potassic and phyllic zones at

Fig. 1 Index map showing the boundaries of geological subdivisions of ZOB (Zagros orogenic belt) and associated porphyry copper deposits in Iran



Dalli porphyry copper deposit, describe the chemical composition by systematic electron-microprobe analyses, and discuss their geochemical and petrological significance by means of the thermodynamic intensive parameters.

Geology and petrography of the Dalli district

The Dalli VPR are emplaced within the central province of Iran, which is situated about 120 km SW of Tehran and 60 km of NE of Arak (Fig. 2). The Dalli porphyry copper prospect area lies near the contact of the UDMA and Sanandaj–Sirjan Zone, which are subdivisions of the Zagros Orogenic Belt and products of the subduction-related closure of the Neo-Tethys Ocean. The area is underlain by the Paleogene andesitic volcanics and pyroclastics and is intruded by the Pliocene lensoid-shaped bodies of diorite, quartz-diorite, tonalite and granodiorite porphyries with calc-alkaline affinity. The oldest unit in this area is red marl, which is interbedded with sandstone, conglomerate, and gypsum. Initial surface sampling, which was carried out to produce the first geological and geochemical reports in the study area and its surroundings recognized a porphyry-type Cu–Au mineralization (Haroni 2005).

The mineralized and altered stock at Dalli is exposed with a surface outcrop of approximately 20 km², which is elongated within 3–4 km long corridor of NE–SW trending and consists of compositionally three different porphyry style intrusive phases. The most intensely mineralized zone occurs within a 200 m wide conical hill, called as the *South Hill*, where the hornblende-bearing diorite forms the dominant rock body (Fig. 2). About 1.7 km distance away from the *South Hill* in NE direction, another intrusive body intruded into the volcanic rocks is exposed in a surface area of over 200×400 m, which is called as the *Central Hill*. The intrusive in *Central Hill* has a core of hornblende- and biotite-bearing tonalite with hornblende-bearing diorite composition to the southern part. To do NE direction, in approximately 1.2 km distance from the *Central Hill*, the third an altered granodiorite intrusive is exposed in which the phyllic zone assemblage constitutes main alteration zone. The area where granodiorite is the dominant rock composition is called as the *North Hill*. The granodiorite intrusive body comprises an area of 80×180 m on surface and it is has intruded into the hornblende- and biotite-bearing tonalite and related volcanic rocks.

In the Dalli area, the calc-alkaline VPR have porphyritic texture and they are composed mainly of biotite, amphi-

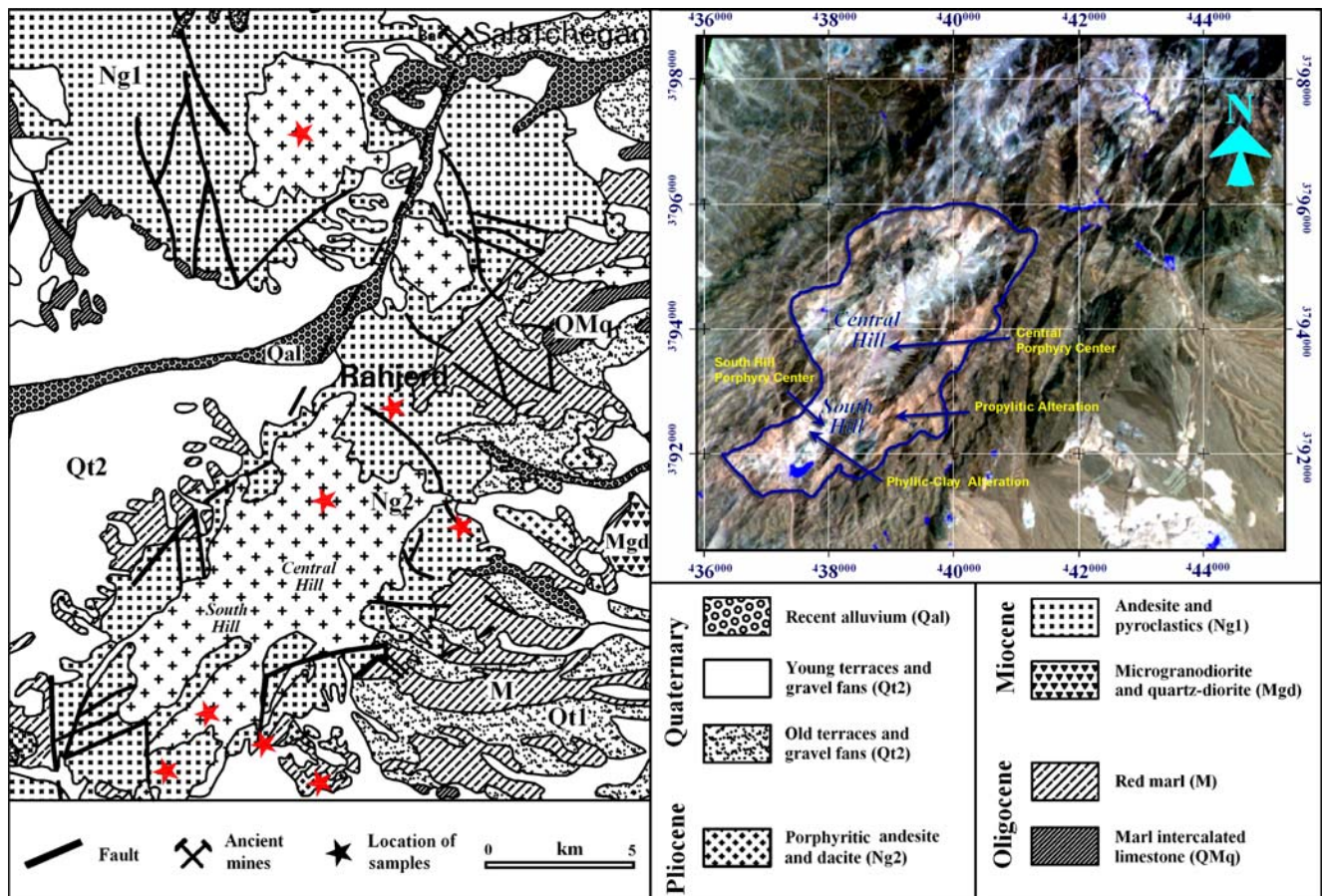


Fig. 2 Simplified geological map of the Dalli area, Arak, central Iran (modified from Emami 1991)

bole, plagioclase, K-feldspar and quartz with variable amounts of opaque minerals including mainly pyrite, chalcopyrite and magnetite. Zircon, apatite, and sphene are found as accessory minerals. Amphibole grains subjected to the potassic and phyllic alteration zones are either partially chloritized or completely recrystallized to secondary biotite; the latter are commonly observed as small aggregate clusters. Euhedral to subhedral mica phenocrysts up to 3 mm in size display khaki to dark brown colors. Euhedral to subhedral amphiboles, displaying blue to green pleochroism, together with plagioclase and minor amount of pyroxene phenocrysts in groundmass yield a porphyritic texture to the VPR. Plagioclase occurs as phenocryst and microphenocryst with variable size and oscillatory zoning.

Mineralization and alteration types

Alteration and mineralization processes in the Dalli porphyry copper system were studied in detail by petrographic techniques and analytical data obtained from electron-microprobe studies for outcrop samples collected particularly in the *South*, *Central*, and *North Hills*. Mineralization occurs as dissemination in altered VPR exposed in the potassic alteration zone and veinlets and fractures within the phyllic alteration zone. Mineralization at the Dalli area are characterized by: (1) gold-rich porphyry style copper deposit associated with porphyritic intrusives, (2) occurrence of hematite and magnetite ores, and (3) widespread quartz–magnetite veins and stockworks. Porphyry style mineralization in Iran occurs within the UDMA with dominant Cu±Mo ore paragenesis. The porphyry-type copper mineralization at Dalli is distinctly Au-rich and high concentrations are found within the porphyritic hornblende-bearing diorite and hornblende- and biotite-bearing tonalite intrusives.

The main porphyry mineralization at Dalli is found within the *South Hill*, which is approximately a lens-like conical hill elongated in NE direction, dipping at 55° to the south, with a length of 225 m and a width of 190 m, and a vertical height of 50 m. The VPR at *South Hill* have been subjected to intensive potassic and phyllic alteration processes. The porphyry system at the *South Hill* consists of moderate to complex stockwork veinlets dominantly with the quartz–magnetite–pyrite–specularite–chalcopyrite assemblage. The density of veinlets system ranges between 10 and 50 per meter. The porphyry system at the *Central Hill* includes quartz–magnetite veinlets ranging from 1 to 10 mm width. The density of veinlets system at the *Central Hill* ranges from 1 to 5 per meter. The intrusive with granodiorite composition at the *North Hill* is elongated in the NE-trending and host dominantly the phyllic and locally

argillic alteration zones with the quartz–chlorite–sericite–clay–limonite–jarosite assemblage. The main hypogene mineralization was developed at the *South Hill* and *Central Hill* within the VPR of Dalli porphyry system. The copper and gold contents of overall Dalli porphyry system are high with an average grade of 0.75% Cu and 1.2 ppm Au, respectively. Mainly three alteration zones have been recognized including potassic, phyllic, propylitic, and locally argillic on the basis of detailed field and laboratory studies. An intense hydrothermal alteration is restricted to the porphyritic biotite- and amphibole-bearing andesite, dacite, diorite and tonalite in the *South* and *Central Hills* (see Fig. 2). Petrographic and electron-microprobe studies show that primary biotite in the least-altered VPR is commonly in the forms of euhedral to subhedral and enriched in Fe with brown to reddish-brown colors (Fig. 3a).

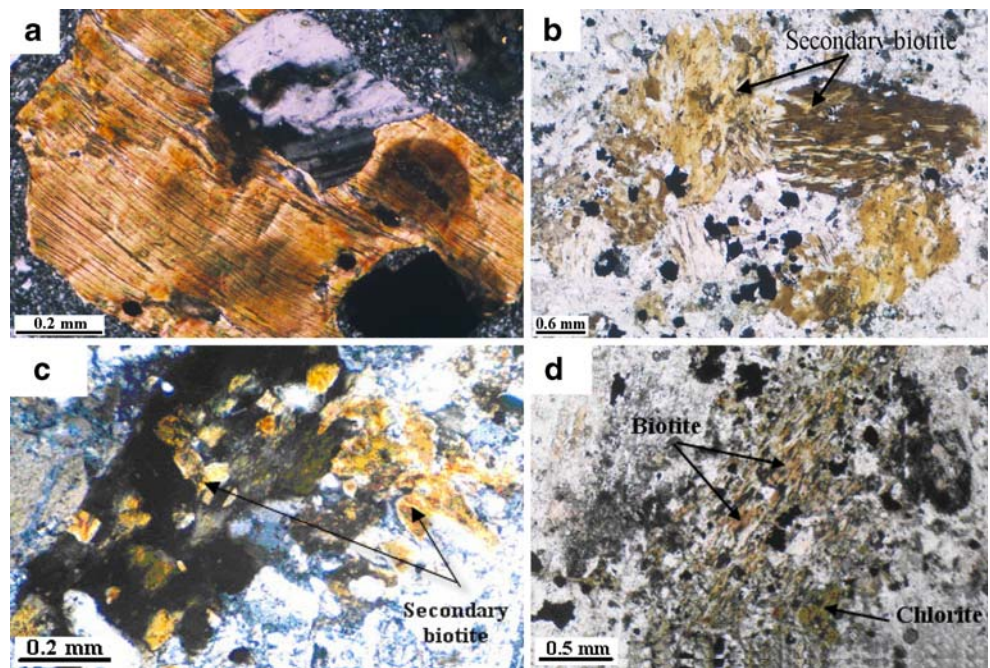
Potassic alteration

On the basis of detailed petrographic studies on rock samples taken from the Dalli area, we have established an extensive potassic alteration zone, which is characterized by the secondary biotite and rare secondary K-feldspar grains. The potassic alteration is manifested by replacement of pre-existent phenocrysts within groundmass or crystallization of secondary veinlets in the VPR. This alteration is represented by the secondary biotite, K-feldspar, quartz, chalcopyrite, pyrite, and magnetite assemblage. Secondary biotites occur as *replacement biotite* in the form of fine-grained flakes or patches, *veinlet biotite*, and *disseminated biotite* throughout the groundmass of VPR. *Replacement biotite* was formed most commonly by the replacement of amphiboles, plagioclase and other ferromagnesian phenocrysts in the matrix of VPR (Fig. 3b,c). This type of biotite is recognized in light brown to dark yellow colors in plane polarized light with mostly unusual sagenetic rutile needles and inclusions. *Veinlet biotite* with its light brown to green colors in plane polarized light makes up as fine-grained subhedral crystals associated commonly with quartz, chlorite, and opaque minerals. *Disseminated biotite* occurs as fine-grained crystals within the groundmass of the VPR. Its color in plane polarized light varies from brownish-yellow to green. The original rock texture is preserved in potassic alteration zone of the VPR.

Phyllic alteration

At Dalli a zone of phyllic alteration was developed at the peripheral of potassic alteration zone. In the VPR, potassic alteration has been overprinted by phyllic alteration zone especially at the vicinity of fault contacts. The phyllic

Fig. 3 Photomicrographs in transmitted light showing biotite from the Dalli porphyry copper deposit. **a** Kinking in biotite phenocryst from the least-altered VPR. **b** Secondary biotite from potassic alteration zone. **c** Secondary biotite after igneous amphibole in potassically altered Dalli volcanic and subvolcanic rocks. **d** Altered biotite with chlorite from phyllic alteration zone



alteration is characterized by the replacement of most of rock-forming silicates such as plagioclase and amphibole by sericite and quartz accompanying with variable amounts of pyrite. In the phyllic alteration zone, plagioclase is mainly altered to sericite, and biotite and amphibole to chlorite (Fig. 3d). These alterations resulted in a color change of the rock surface from relatively dark grey to light grey and light green. Pyrite in phyllic alteration zone constitutes the 2–4 vol.% of rock and forms as disseminations and veinlets within the groundmass of VPR. Silicification is an extensive phenomenon in this alteration zone that lends a bleached white color to the rocks.

Propylitic and argillic alterations

Propylitic alteration is distal to the core potassic and its peripheral phyllic alteration zones and forms a halo around the mineralized potassic zone. It is characterized by occurrence of epidote, chlorite, calcite, and locally actinolite. These alteration minerals formed by most commonly the replacement of primary amphibole and plagioclase in the groundmass of VPR. Chloritization of the primary amphibole phenocrysts is pervasive. Biotite phenocrysts are partially altered to epidote, chlorite, and sericite. Locally, the argillic has preferentially developed in the Dalli area along fissures and faults. The VPR in the argillic zone are very soft, light brown to yellow colors, and characterized by jarosite, which is commonly associated with hematite, limonite and clay minerals. The primary rock textures in argillic zone are totally obscured. Field observations indicate that local argillic alteration assemblages are

adjacent to the phyllic alteration zone. Disseminated pyrite is widespread in the argillic alteration zone.

Analytical techniques

Micas and chlorites were analyzed in the Electron Microprobe Laboratory of Oklahoma University in USA. Electron-microprobe analyses were performed on a Cameca SX50 at OU, equipped with 5 asynchronous wavelength dispersive spectrometers and PGT PRISM2000 energy dispersive X-ray detector. The analytical conditions were 20 kV acceleration voltage, 20 nA sample current, and 3- μ m spot size. K-alpha emissions were acquired for all elements except for Ba in which the L-alpha emission is used. Counting times were 30 s on peak for all elements, yielding calculated minimum levels of detection (at 3-sigma above mean background) of ≤ 0.02 wt.% of the oxide for all components except for Ba (0.09 wt.% BaO) and F (0.10 wt. %). Natural minerals and synthetic/compound were used as standards. Representative mica and chlorite analyses from the potassic and phyllic alteration zones at Dalli porphyry copper deposit are given in Table 1 and Table 2, respectively. Mica recalculation scheme together with the end-member names, mole fractions, ferric and ferrous iron estimation on the basis of stoichiometric constraints, fluorine and chlorine intercept values, biotite geothermometer and fugacity ratios is carried out by Mica⁺ program (Yavuz 2003a). The *Chlorite Formula Unit Calculator and Variety Namer* Excel spreadsheet developed by Tindle AG is used for the calculation of the structural formulas.

Results

Biotite mineral chemistry

A total of 95 electron-microprobe biotite analyses were obtained from the VPR at Dalli porphyry copper deposit. Representative biotite analyses from the potassic and phyllic zones are given in Table 1. According to the nomenclature of Foster (1960) for the classification of trioctahedral micas by chemical and lithological affinity, biotites from the potassic and phyllic zones at Dalli area plot in the Mg biotites field of $Mg-(Al^{VI}+Fe^{3+}+Ti)-(Fe^{2+}+Mn)$ ternary diagram (Fig. 4a). Composition of studied biotite on *mgli* (Mg–Li) vs. *feal* ($Fe_{tot}+Mn+Ti-Al^{VI}$) diagram of Tischendorf et al. (1997), which provides a simple means to classify micas in terms of chemical composition and site occupancy, also plot dominantly in Mg biotite field (Fig. 4b). In the trioctahedral mica quadrilateral, biotite from the potassic and phyllic zones show a distinct variation plotting in eastonite and phlogopite fields (Fig. 4c). In the Dalli area, biotites in potassic zone have a low Al (*apfu*) total contents compared to biotites in the phyllic alteration assemblages (Fig. 5a). The Fe (*apfu*) content of biotites describes a distinctive variation from higher Fe values at the potassic zone to lower Fe contents in the phyllic alteration assemblage (Fig. 5b). Biotite from the potassic zone contains higher K (*apfu*) values than the phyllic alteration assemblage (Fig. 5c). The Na (*apfu*) content of biotite displays a gradual decrease from the potassic zone to the phyllic zone. The Ba (*apfu*) content of biotite from the potassic alteration zone displays mainly two populations. In general, the Ti (*apfu*) content of biotite at potassic zone describes an enrichment trend when compared to Ti content of biotite in phyllic zone. At Dalli porphyry copper deposit, the F (wt.%) and Cl (wt.%) contents of biotite exhibit no significant differences in the potassic and phyllic alteration assemblages. Although, the F (wt.%) content of biotite in the potassic and phyllic alteration assemblages describes a similar trend, it seems that the Cl (wt.%) content of biotite from the phyllic alteration zone display slightly higher values. Variation of some of oxide contents of biotites vs. mole fraction of Mg (X_{Mg}) is shown in Fig. 6. The X_{Mg} is positively correlated with Al_2O_3 , (K_2O+Na_2O+BaO) , and F, but negatively correlated with FeO and TiO_2 contents of biotite in the potassic zone. On the other hand, the X_{Mg} is positively correlated with FeO, (K_2O+Na_2O+BaO) , and TiO_2 , but negatively correlated with Al_2O_3 and Na_2O contents in the phyllic alteration zone.

Biotite halogen chemistry

The halogen chemistry of biotite from the phyllic and potassic alteration zones at Dalli is estimated by Mica⁺

program (Yavuz 2003a). The Cl (wt.%) content of Dalli biotites correlates positively with the mole fraction of Mg (X_{Mg}) in the phyllic and potassic alteration zones and contrasts to “Mg–Cl avoidance” in the phyllic–potassic alteration at the Santa Rita porphyry copper deposit. Compared to the F content, the amount of Cl substitution in the OH site is much less with a few exceptional biotites having $Cl/(OH+F+Cl)$ greater than 0.1 (Munoz 1984). Similar positive trend also is observed in the F (wt.%) vs. X_{Mg} content of biotites in the potassic alteration zone. The positive correlation between high X_{Mg} and F (wt.%) values is called as “Fe–F avoidance” and obvious in biotites from the potassic alteration zone of classical porphyry copper deposits. Munoz (1984) pointed out that the Cl (wt.%) and F (wt.%) contents of biotite may not be used alone to deduce the relative halogen fugacities in the associated fluids. This means that biotites with the same Cl (wt.%) and F (wt.%) contents may not inevitably crystallize from fluids with the same relative HCl and HF fugacities.

Biotites from the phyllic and potassic alteration zones have, in general, similar F/(F+Cl) ratios. Positive correlation between the X_{Mg} and Cl (wt.%) in biotites from the phyllic zone is shifted to negative correlation between the X_{Mg} and F/(F+Cl) ratios. This may point out that the Mg and Fe content of biotites in the phyllic alteration is directly related to F–Cl–OH exchange between mica chemistry and hydrothermal fluids. The fluorine intercept [IV (F)], chlorine intercept [IV (Cl)], and F/Cl intercept [IV (F/Cl)] values are important physicochemical parameters to describe the relative degree of F and Cl contents in mica, which are all related to the fugacity ratios of f_{HCl}/f_{HF} . These values are defined by Munoz (1984) as:

$$IV(F) = 1.52X_{Mg} + 0.42X_{An} + 0.20X_{Sid} - \log(X_F/X_{OH}) \quad (1)$$

$$IV(Cl) = -5.01 - 1.93X_{Mg} - \log(X_{Cl}/X_{OH}) \quad (2)$$

$$IV(F/Cl) = IV(F) - IV(Cl) \quad (3)$$

where

$$X_{Sid} = [(3 - Si/Al)/1.75] \times (1 - X_{Mg}) \quad (4)$$

$$X_{An} = 1 - (X_{Mg} + X_{Sid}) \quad (5)$$

Biotite compositions from the potassic and phyllic alteration zones are shown in Fig. 7 plotted with respect to IV (F) vs. IV (F/Cl). In this figure, the values on the axes

Table 1 Representative electron-microprobe analyses of hydrothermal biotite from the Dalli porphyry copper deposit

	Biotite from potassic zone						Biotite from phyllic zone			
	1	2	3	4	5	7	8	9	10	11
SiO ₂	37.29	37.09	37.85	37.39	36.99	37.51	39.32	40.31	41.15	42.16
TiO ₂	4.52	4.54	4.7	4.65	5.07	4.93	3.82	3.97	4.08	3.54
Al ₂ O ₃	13.16	13.47	13.33	13.61	13.06	13.47	14.6	14.22	14.38	15.36
FeO _{tot}	13.3	13.32	12.94	13.42	13.07	13.36	11.39	11.05	11.13	11.43
MnO	0.25	0.24	0.23	0.24	0.23	0.27	0.06	0.03	0.02	0.05
MgO	15.83	16.52	16.26	16.12	15.82	16.14	13.46	13.41	13.31	12.76
CaO	0.03	0.04	0.02	0.01	0.1	0.02	0.15	0.17	0.12	0.11
Na ₂ O	0.33	0.36	0.26	0.25	0.3	0.31	0.15	0.16	0.16	0.17
K ₂ O	8.81	8.81	9.23	9.25	8.35	8.92	5.8	5.48	6.56	6.29
BaO	0.79	0.81	0.27	0.25	0.74	0.96	0.43	0.37	0.42	0.2
F	0.6	0.63	0.49	0.52	0.48	0.44	0.65	0.82	0.61	0.59
Cl	0.3	0.29	0.26	0.24	0.26	0.23	0.37	0.32	0.35	0.3
O=F, Cl	0.32	0.33	0.26	0.27	0.26	0.24	0.36	0.42	0.34	0.32
Total	94.89	95.79	95.58	95.68	94.21	96.32	89.84	89.89	91.95	92.64
Si	2.812	2.773	2.816	2.788	2.798	2.786	3.003	3.059	3.065	3.096
Al	1.170	1.187	1.169	1.196	1.164	1.179	1.315	1.271	1.263	1.329
Ti	0.256	0.255	0.263	0.261	0.288	0.275	0.219	0.227	0.229	0.195
Fe	0.838	0.833	0.805	0.837	0.826	0.83	0.728	0.701	0.694	0.702
Mn	0.016	0.015	0.014	0.015	0.015	0.017	0.004	0.002	0.001	0.003
Mg	1.780	1.841	1.803	1.792	1.784	1.787	1.533	1.517	1.478	1.397
Ca	0.002	0.003	0.002	0.001	0.008	0.002	0.012	0.014	0.01	0.009
Na	0.048	0.052	0.038	0.036	0.044	0.045	0.022	0.024	0.023	0.024
K	0.848	0.84	0.876	0.88	0.806	0.845	0.565	0.53	0.623	0.589
Ba	0.023	0.024	0.008	0.007	0.022	0.028	0.013	0.011	0.012	0.006
OH	1.818	1.814	1.852	1.847	1.852	1.868	1.795	1.762	1.812	1.826
F	0.143	0.149	0.115	0.123	0.115	0.103	0.157	0.197	0.144	0.137
Cl	0.038	0.037	0.033	0.03	0.033	0.029	0.048	0.041	0.044	0.037
X _{Mg}	0.680	0.688	0.691	0.682	0.684	0.683	0.678	0.684	0.680	0.666
X _{Fe}	0.320	0.312	0.309	0.318	0.316	0.317	0.406	0.405	0.409	0.447
Charge +	22.127	22.222	22.138	22.188	22.202	22.174	21.843	21.785	21.898	22.048
Ph	0.581	0.592	0.585	0.581	0.58	0.578	0.5	0.492	0.482	0.451
Ann	0.147	0.113	0.131	0.127	0.108	0.123	0.217	0.224	0.185	0.147
PDO	0.183	0.207	0.194	0.202	0.213	0.204	0.107	0.103	0.151	0.201
Tib	0.084	0.082	0.085	0.085	0.094	0.089	0.072	0.073	0.075	0.063
Mnb	0.005	0.005	0.005	0.005	0.005	0.005	0.001	0.001	0	0.001
Alb	0	0	0	0	0	0	0.104	0.107	0.107	0.137
Phlogopite	19.525	6.401	17.76	12.751	0	8.465	2.380	1.288	9.072	0
Ti-phlogopite	25.636	25.528	26.296	26.072	28.199	27.538	21.943	22.655	22.858	18.909
Ferri-eastonite	38.75	48.036	40.044	44.516	49.436	44.969	6.19	1.073	12.581	24.537
Muscovite	8.257	11.985	8.201	9.066	11.724	10.97	1.032	0.179	10.484	19.777
Eastonite	0	0	0	0	0	0	29.71	32.691	11.846	1.589
Talc	7.833	8.05	7.699	7.595	11.746	8.058	38.745	42.114	33.158	35.992
IV (F)	2.131	2.123	2.238	2.202	2.234	2.279	1.983	1.875	2.013	1.994
IV (Cl)	-4.455	-4.46	-4.387	-4.348	-4.385	-4.316	-4.401	-4.327	-4.327	-4.191
IV (F/Cl)	6.586	6.582	6.626	6.55	6.618	6.595	6.383	6.202	6.34	6.185
log (X _{Cl} /X _{OH})	-1.676	-1.693	-1.752	-1.785	-1.745	-1.81	-1.574	-1.632	-1.613	-1.689
log (X _F /X _{OH})	-1.104	-1.085	-1.206	-1.178	-1.207	-1.257	-1.058	-0.952	-1.1	-1.124
log (X _F /X _{Cl})	0.572	0.608	0.546	0.607	0.537	0.553	0.516	0.68	0.512	0.565
log (fH ₂ O)/(fHF)	5.814	5.813	5.922	5.889	5.916	5.963	6.387	6.266	6.396	6.363
log (fH ₂ O)/(fHCl)	4.446	4.473	4.526	4.555	4.514	4.578	4.644	4.695	4.667	4.715
log (fHF)/(fHCl)	-2.276	-2.267	-2.312	-2.243	-2.309	-2.29	-2.664	-2.479	-2.618	-2.48
Biotite geothermometer (°C)	427	442	433	428	426	424	341	334	325	300

The crystallo-chemical formulae were calculated on the basis of 22 cation charges by using Mica⁺ program (Yavuz 2003a). The *Ph* (phlogopite), *Ann* (annite), *PDO* (proton-deficient oxyannite), *Tib* (titanobiotite), *Mnb* (manganobiotite) and *Alb* (aluminobiotite) are mole fractions, determined on basis of octahedral ions (calculations from Jacobs and Parry 1979). The X_{Mg} ($X_{Mg} = Mg/(Mg+Fe)$) and X_{Fe} ($X_{Fe} = (Fe+Al^{VI})/(Fe+Mg+Al^{VI})$) values are mole fractions of Mg and Fe (from Zhu and Sverjensky 1992). Mica end-member calculation as Phlogopite, Ti-phlogopite, Ferri-eastonite, Muscovite, Eastonite, and Talc is taken from Dymek (1983). Methods of fluorine IV (*F*), chlorine IV (*Cl*), and fluorine/chlorine IV (*F/Cl*) intercept values are from Munoz (1984). The fugacity ratios of $\log (fH_2O)/(fHF)$, $\log (fH_2O)/(fHCl)$, and $\log (fHF)/(fHCl)$ are calculated using the equations by Munoz (1992). Calculating method for biotite geothermometer is from Beane (1974). Ferric iron estimations as PDO are from Dymek (1983).

Table 2 Representative electron-microprobe analyses of chlorite in the Dalli porphyry copper deposit

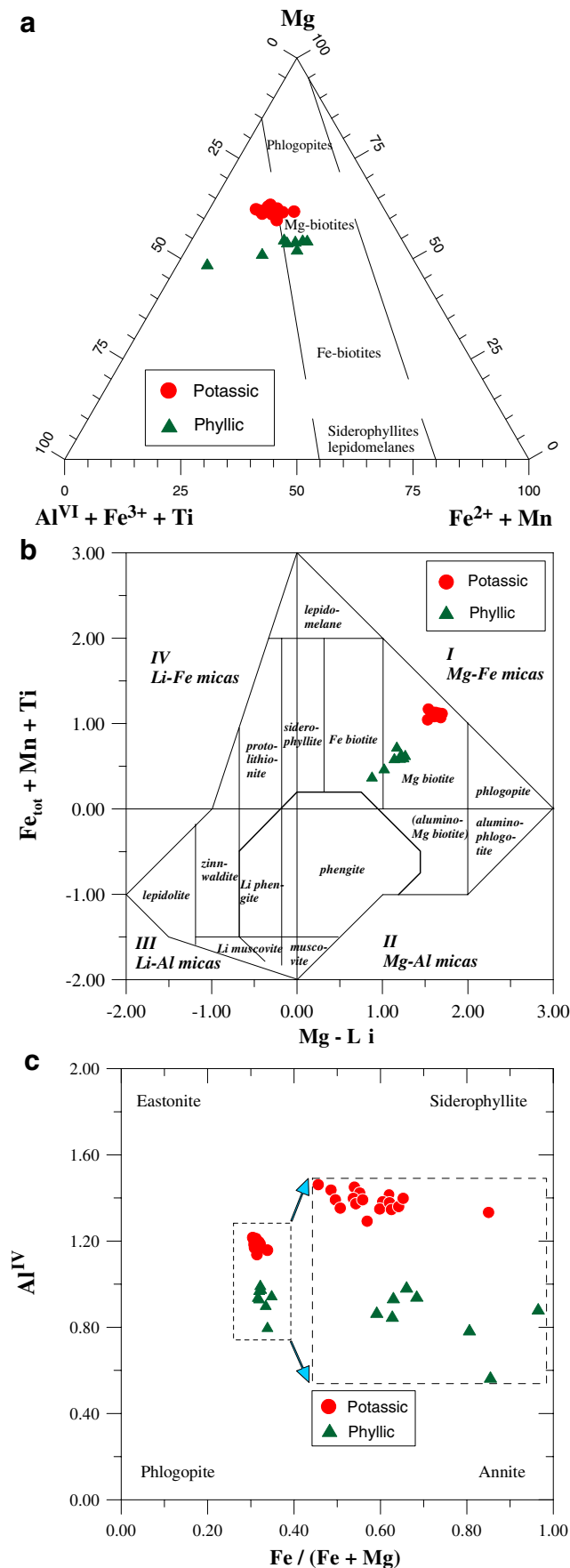
	Replacement chlorite from hydrothermal biotite			Veinlet chlorite	
	1	2	3	4	5
SiO ₂	28.64	27.21	29.17	30.08	30.37
TiO ₂	0.07	0.1	0.02	0.07	0.07
Al ₂ O ₃	21.14	20.47	20.38	21.00	20.84
FeO _{tot}	20.80	22.10	20.26	17.90	17.16
MnO	0.55	0.66	0.48	0.38	0.34
MgO	15.69	16.57	15.74	14.86	16.66
CaO	0.04	0.04	0.03	0.06	0.06
Na ₂ O	0.00	0.00	0.00	0.02	0.01
K ₂ O	0.01	0.01	0.02	0.07	0.01
BaO	0.00	0.00	0.05	0.00	0.03
F	0.31	0.21	0.45	0.47	0.58
Cl	0.01	0.01	0.02	0.01	0.00
O=F, Cl	0.13	0.09	0.19	0.20	0.24
Total	87.48	87.44	86.84	85.30	86.44
H ₂ O ^(*)	11.36	11.32	11.16	11.12	11.22
Total	98.84	98.76	98.00	96.42	97.66
Si	5.795	5.610	5.907	6.070	6.024
Al ^{IV}	2.205	2.390	2.093	1.930	1.976
Al ^{VI}	2.904	2.618	2.852	3.177	3.001
Ti	0.011	0.016	0.003	0.011	0.010
Fe ^{(3+)*}	0.531	0.235	0.618	0.892	0.819
Fe ^{(2+)*}	2.988	3.575	2.813	2.129	2.028
Mn	0.094	0.115	0.082	0.065	0.057
Mg	4.733	5.092	4.751	4.47	4.926
Ca	0.009	0.009	0.007	0.013	0.013
Na	0.000	0.000	0.000	0.016	0.008
K	0.005	0.005	0.010	0.036	0.005
Ba	0.000	0.000	0.008	0.000	0.005
F	0.397	0.274	0.576	0.600	0.728
Cl	0.007	0.007	0.014	0.007	0.000
OH ^(*)	15.596	15.719	15.410	15.393	15.272
Total	35.275	35.666	35.144	34.809	34.871
Fe/(Fe+Mg)	0.427	0.428	0.419	0.403	0.366
Variety	<i>Pycnochlorite</i>	<i>Pycnochlorite</i>	<i>Pycnochlorite</i>	<i>Pycnochlorite</i>	<i>Pycnochlorite</i>
Chlorite geothermometry (°C)	293	323	275	249	256

The crystallo-chemical formulae were calculated on the basis of 28 oxygens. Chlorite recalculation with Fe^{(3+)*}, Fe^{(2+)*} and H₂O^(*) estimation is carried out by *Chlorite Formula Unit Calculator and Variety Namer* Excel spreadsheet written by *Tindle AG*. Chlorite geothermometry is from Cathelineau (1988).

increase upward and to the right with a high correlation coefficient ($r=0.93$). A compositional distinction is not evident between biotite varieties, but it seems that biotites from the potassic alteration zone have higher IV (F) and IV (F/Cl) values than biotite grains from the phyllic alteration zone. Loferski and Ayuso (1995) attributed this situation in mica composition to the crystal fractionation process. The relative degree of Cl and F enrichments in mica is expressed with a single numerical value proposed by Munoz (1984). The fluorine IV (F), chlorine IV (Cl), and IV (F/Cl) intercept values for micas from barren and ore-related magmatic rocks can be used as an important parameter to express the relative degree of F and Cl contents in mica, and relate to the fugacity ratio of $f_{\text{HCl}}/f_{\text{HF}}$. Histograms of the IV (F), IV (Cl), and IV (F/Cl)

intercept values calculated from the halogen contents of biotite from potassic and phyllic alteration zones at Dalli porphyry copper deposit are given in Fig. 8. Biotite grains have IV (Cl) values of -4.49 to -4.17 (mean= -4.35 , see Fig. 8a), IV (F) values of 1.78 to 2.52 (mean= 2.09 , see Fig. 8b), and IV (F/Cl) values of 5.95 to 6.90 (mean= 6.44 , see Fig. 8c). These ranges at Dalli are consistent with the extent of intercept values of biotites from other well-known worldwide porphyry copper deposits (Taylor 1983; Munoz 1984; Loferski and Ayuso 1995; Selby and Nesbitt 2000; Yavuz 2003b) for IV (F) (1.1 to 3.0), IV (Cl) (-5.0 to -2.7), and IV (F/Cl) (4.60 to 7.0) values.

Zhu and Sverjensky (1992) showed that biotites formed under the similar T , P , and fluid composition display linear trends on $\log(X_{\text{Cl}}/X_{\text{OH}})$ vs. X_{Mg} , $(X_{\text{F}}/X_{\text{OH}})$ vs. X_{Fe} , and \log



◀ **Fig. 4** **a** Plot of biotites from the potassic and phyllic zones in Dalli porphyry copper deposit in the ternary Mg–(Fe²⁺+Mn)–(Al^{VI}+Fe³⁺+Ti) diagram of Foster (1960). **b** Chemical compositions of biotites on the (Mg–Li) vs. (Fe_{tot}+Mn+Ti–Al^{VI}) classification diagram of Tischendorf et al. (1997). **c** plot of Fe/(Fe+Mg) vs. Al^{IV} in biotite from the Dalli area

(X_F/X_{Cl}) vs. X_{Fe} plots. The slopes of these linear trends are only a function of T , but the intercept values are functions of physicochemical conditions such as T , P , and fluid compositions. The halogen content of biotite grains in terms of $\log(X_{Cl}/X_{OH})$ and $\log(X_F/X_{OH})$ ratios from the potassic and phyllic alteration zones at Dalli is shown in Fig. 9. These $\log(X_{Cl}/X_{OH})$ and $\log(X_F/X_{OH})$ ratios range from -1.81 to -1.66 (mean= -1.75) and -1.69 to -1.57 (mean= -1.63) for the potassic, and -1.49 to -0.99 (mean= -1.20) and -1.15 to -0.93 (mean= -1.06) for the phyllic alteration zones. In $\log(X_{Cl}/X_{OH})$ vs. X_{Fe} plot (Fig. 9a); the halogen content of biotite from the potassic and phyllic alteration zones defines linear trends without a broad scatter. The y -intercepts on the $\log(X_{Cl}/X_{OH})$ vs. X_{Fe} plot for biotites from the potassic and phyllic zones display a similar range with -1.09 and -1.20 , respectively. In the $\log(X_{Cl}/X_{OH})$ vs. X_{Mg} plot (Fig. 9c); the (X_{Cl}/X_{OH}) ratio scatters in a narrow range with the y -intercept values of -3.15 and -2.87 for potassic and phyllic zones, respectively. Selby and Nesbitt (2000) attributed the similarity of intercepts and narrow scatter for halogen content of biotite in the potassic and phyllic alteration zones from the Casino porphyry Cu–Au–Mo mineralization, Yukon, Canada to the constant (X_F/X_{OH}) and (X_{Cl}/X_{OH}) values of hydrothermal fluid with broadly similar temperature conditions. The $\log(X_{F1}/X_{OH})$ vs. X_{Fe} and (X_{F1}/X_{OH}) vs. X_{Mg} plots of the halogen content of biotite from the potassic and phyllic zones at Dalli show different trends when compared to the (X_{Cl}/X_{OH}) vs. X_{Fe} and (X_{Cl}/X_{OH}) vs. X_{Mg} plots. The y -intercepts on the $\log(X_{F1}/X_{OH})$ vs. X_{Fe} and $\log(X_{F1}/X_{OH})$ vs. X_{Mg} plots (Fig. 9b, d) for biotites from the potassic and phyllic zones are 0.48 , -1.54 and -5.83 , -1.13 , respectively. The $\log(X_{Cl}/X_{OH})$ vs. X_{Fe} and X_{Mg} plots produced approximately linear trends for the Cl content of biotite from the potassic and phyllic alteration zones at Dalli porphyry copper deposit. The similar intercept values and the narrow scatter for the $\log(X_{Cl}/X_{OH})$ ratios may suggest that the hydrothermal fluid, which is responsible for the potassic and phyllic alteration zones at Dalli were nearly constant under relatively similar temperature conditions. The scatter in $\log(X_F/X_{OH})$ ratios with respect to the estimated slopes (see Fig. 9b,d) is the evidence of biotite formed under dissimilar composition and temperature conditions in the potassic and phyllic alteration zones. This contrast in biotite composition also is reflected by the consistent and inconsistent situations in Fe–F and Mg–Cl avoidance rules in phyllic and potassic alteration zones at Dalli porphyry copper deposit.

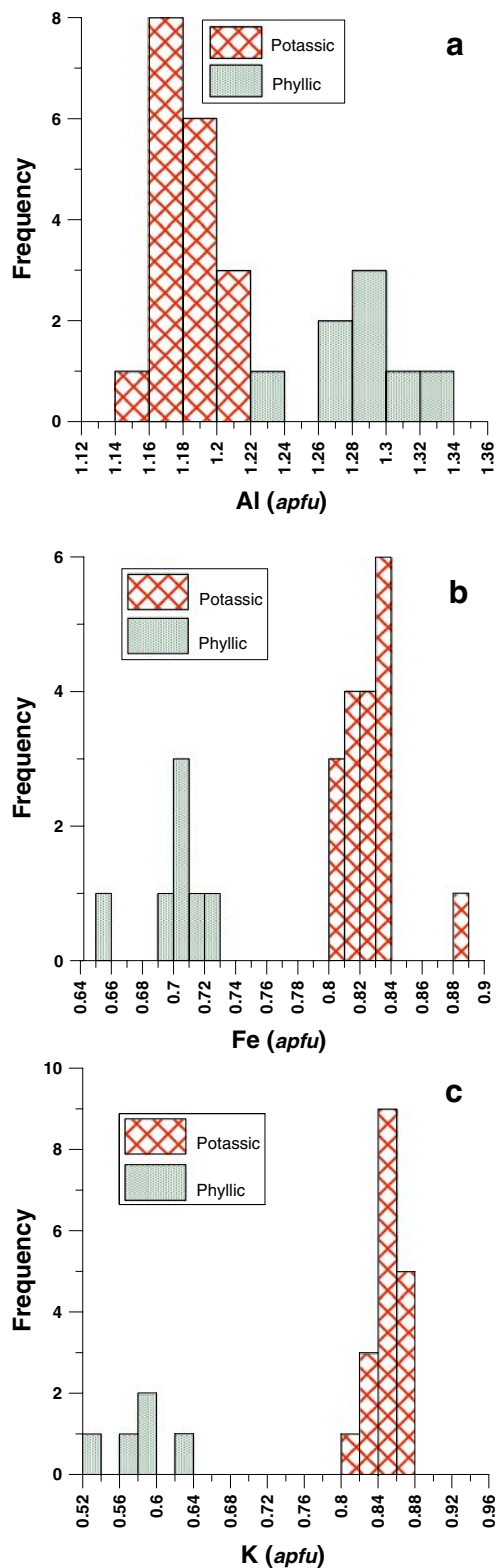


Fig. 5 Histograms of electron-microprobe biotite chemistry from the potassic and phyllic alteration zones for **a**) Al (apfu), **b**) Fe (apfu), and **c**) K (apfu)

Hydrothermal fluid fugacity ratios and comparison with other porphyry Cu±Mo systems

Fluorine and chlorine data in biotite were used to estimate the $\log(f\text{H}_2\text{O}/f\text{HF})$, $\log(f\text{H}_2\text{O}/f\text{HCl})$, and $\log(f\text{HF}/f\text{HCl})$ ratios for hydrothermal fluids, which are responsible for the mineralization and hydrothermal alteration processes at Dalli porphyry copper deposit. The fugacity ratios were estimated by using the equations proposed by Munoz (1992), which are based on the revised coefficients for F–Cl–OH partitioning between biotite and hydrothermal fluid (Zhu and Sverjensky 1991, 1992). These equations are:

$$\log(f\text{H}_2\text{O}/f\text{HF})^{\text{fluid}} = 1,000/T \left(2.37 + 1.1(X_{\text{Mg}})^{\text{biotite}} \right) + 0.43 - \log(X_{\text{F}}/X_{\text{OH}})^{\text{biotite}} \quad (6)$$

$$\log(f\text{H}_2\text{O}/f\text{HCl})^{\text{fluid}} = 1,000/T \left(1.15 + 0.55(X_{\text{Mg}})^{\text{biotite}} \right) + 0.68 - \log(X_{\text{Cl}}/X_{\text{OH}})^{\text{biotite}} \quad (7)$$

$$\log(f\text{HF}/f\text{HCl})^{\text{fluid}} = -1,000/T \left(1.22 + 1.65(X_{\text{Mg}})^{\text{biotite}} \right) + 0.25 - \log(X_{\text{F}}/X_{\text{Cl}})^{\text{biotite}} \quad (8)$$

where X_{F} , X_{Cl} , and X_{OH} are the mole fractions of F, Cl, and OH in the hydroxyl site of biotite, $(X_{\text{Mg}})^{\text{biotite}}$ is the sum of Mg/sum octahedral cations, and T is the temperature in Kelvin of the halogen exchange. Biotites from the potassic and phyllic alteration zones have $\log(f\text{HF}/f\text{HCl})$ values of -2.60 to -2.07 (mean= -2.31) and -2.70 to -2.25 (mean= -2.55), $\log(f\text{H}_2\text{O}/f\text{HF})$ values of 5.69 to 6.21 (mean= 5.91) and 6.12 to 6.47 (mean= 6.35), and $\log(f\text{H}_2\text{O}/f\text{HCl})$ values of 4.44 to 4.58 (mean= 4.52) and 4.64 to 4.72 (mean= 4.68), respectively. The recalculated fugacity ratios from biotites at Dalli potassic and phyllic alteration zones are compared with the fugacity ratios of other porphyry copper deposits such as Bakırçay (Taylor 1983), Bingham (Parry et al. 1978; Lainer et al. 1978; Bowman et al. 1987), Casino (Selby and Nesbitt 2000), Deboullie (Loferski and Ayuso 1995), Hanover (Jacobs and Parry 1979), Los Pelambres (Taylor 1983), and Santa Rita (Parry et al. 1978). Hydrothermal fluids associated with the potassic and phyllic alteration processes at Dalli were possessed of similar $\log(f\text{H}_2\text{O}/f\text{HF})$ values those with the estimated values for Bingham, Deboullie, Hanover, Los Pelambres, and Santa Rita (Fig. 10a). Hydrothermal fluids, which are responsible for Au-rich porphyry copper deposit at Dalli also have $\log(f\text{H}_2\text{O}/f\text{HCl})$ values typically similar and within the range of Bingham porphyry copper deposit (Fig. 10a). The $\log(f\text{HF}/f\text{HCl})$ values estimated for hydrothermal fluids associated with potassic and phyllic

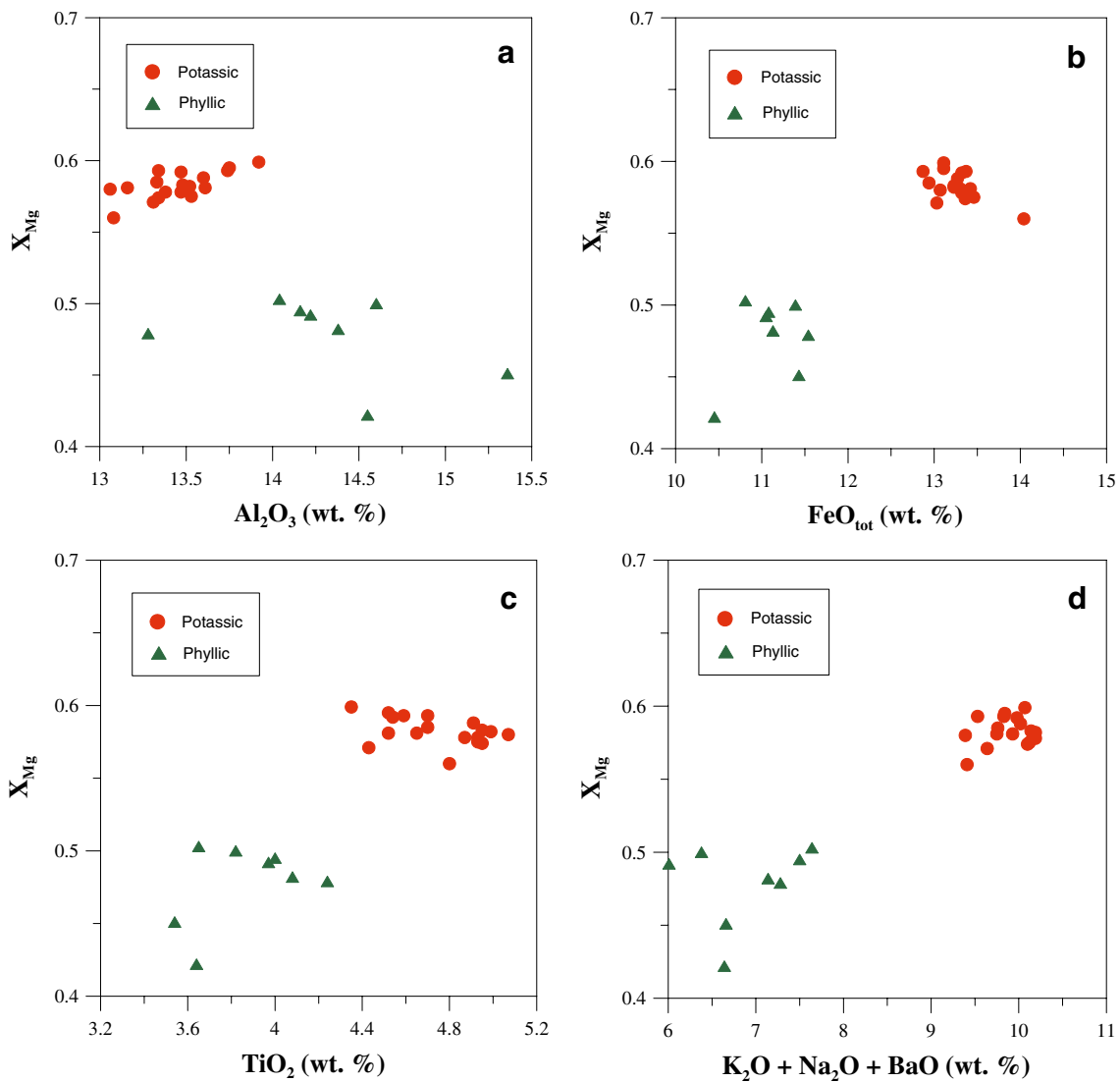


Fig. 6 Compositions of biotite from the potassic and phyllic alteration zones on **a**) X_{Mg} vs. Al_2O_3 (wt. %), **b**) X_{Mg} vs. FeO_{tot} (wt. %), **c**) X_{Mg} vs. TiO_2 (wt. %), and **d**) X_{Mg} vs. $(K_2O + Na_2O + BaO)$ (wt. %) plots

alteration at Dalli differ from those of selected other porphyry Cu deposits. Among the compared fugacity ratios obtained from biotite composition from porphyry copper deposits, the $\log (f_{HF}/f_{HCl})$ fugacity ratios determined for Deboullie, Casino and Bakırçay exhibit more negative values than those from the $\log (f_{HF}/f_{HCl})$ fugacity ratios at Bingham, Hanover, Los Pelambres and Santa Rita. The Dalli porphyry system with its the most negative $\log (f_{HF}/f_{HCl})$ fugacity ratios contrasts greatly with those of the other porphyry Cu deposits, except for Deboullie (Fig. 10b).

Mineral geothermometry

By applying different geothermometers to the recalculated structural formulae of alteration minerals, the formation conditions and crystallization temperatures can be estimated empirically. Biotite geothermometer proposed by Beane

(1974) for hydrothermal biotites in the potassic alteration zone of the North American porphyry copper deposits including Santa Rita, Ray, Safford, Bingham, Hanover, and Galore Creek is applied to biotite from the potassic and phyllic alteration zones of Dalli porphyry copper deposit, where compositions of hydrothermal biotite coexist with magnetite and K-feldspar assemblage. Temperatures determined for the phyllic alteration lie within the range of 280° to 344°C with a mean value of 323°C. The potassic alteration zone is characterized by the higher temperatures at Dalli ranging from 402° to 450°C (mean=430°C). The application of the biotite geothermometer of Beane (1974) to biotites from the potassic alteration zone at Dalli porphyry copper deposit yielded similar temperature range those with the Santa Rita, Ray and Safford (350°–410°C), and Bingham (327°–512°C) and Galore Creek (450°–550°C; Fig. 11).

Petrographic determinations between chlorite and other alteration minerals within the potassic and phyllic alteration zones at Dalli show that an appearance of chlorite was started towards the end of potassic alteration stage and continued progressively in the course of phyllic alteration stage. The Chlorite formation is formed most commonly as a replacement occurrence from hydrothermal biotite in the potassic zone. The development of chlorite in the phyllic zone is found, in general, as veinlets within the groundmass of the VPR. The chemical composition of chlorites from the potassic and phyllic alteration zones at Dalli porphyry copper deposit is given in Table 2. The chlorites are classified according to their dominant divalent cation and compositionally as pycnochlorites according to Hey (1954) or clinochlore according to the International Association for the Study of Clays nomenclature scheme (Bailey 1980). Replacement chlorites within the potassic zone are characterized by relatively higher Fe/(Fe+Mg) ratios (0.42 to 0.43) than the veinlets chlorite (0.37–0.40) in the phyllic alteration zone. In literature, numerous chlorite geothermometers with different correction factors were proposed to estimate the crystallization temperature of chlorites. The application of chlorite geothermometer by Cathelineau (1988) to the chlorites at Dalli porphyry copper deposit yielded temperatures between 275° and 323°C for potassic and 249° and 256°C for phyllic alteration zones.

Summary

All known porphyry style copper deposits in Iran are associated with the Neogene subvolcanic granitoids

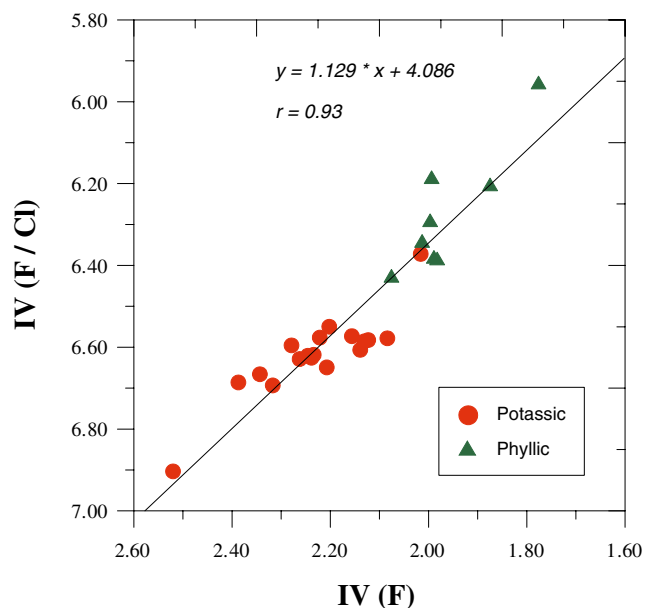


Fig. 7 Plot for IV (F/Cl) vs. IV (F) of biotites at Dalli porphyry copper deposit

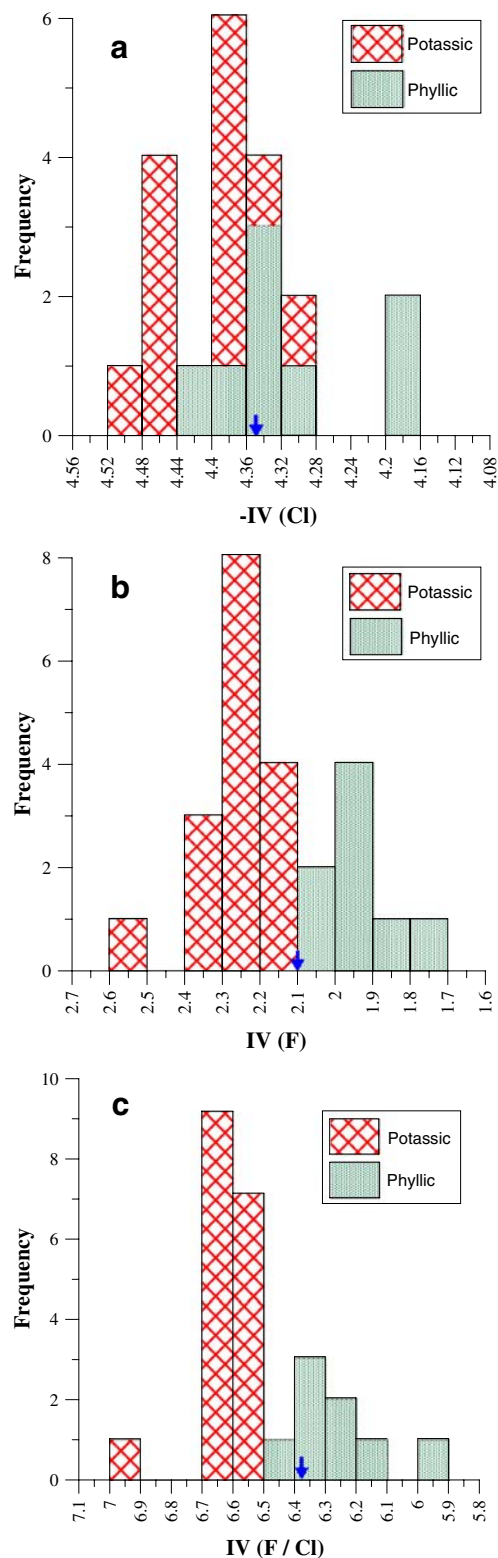


Fig. 8 Histograms of a) chlorine [-IV (Cl)], b) fluorine [IV (F)], and c) F/Cl intercept values [IV (F/Cl)] for biotites from the Dalli porphyry copper deposit. Rows show the mean values of each intercept values

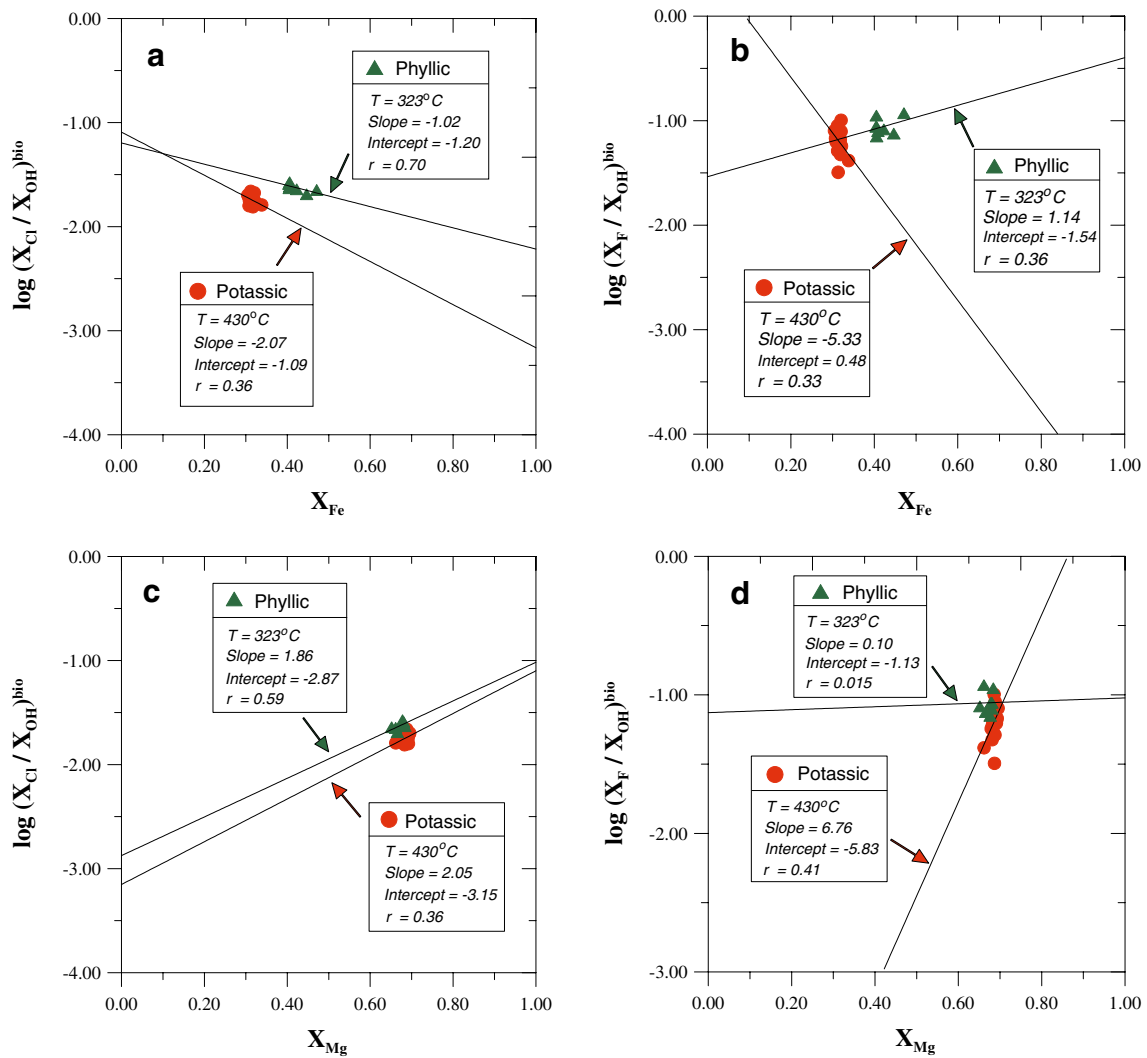


Fig. 9 a, b X_{Fe} vs. $\log(X_{Cl}/X_{OH})$ and $\log(X_F/X_{OH})$, and c, d X_{Mg} vs. $\log(X_{Cl}/X_{OH})$ and $\log(X_F/X_{OH})$, plots of biotites from the potassic and phyllic alteration zones at Dalli porphyry copper deposit

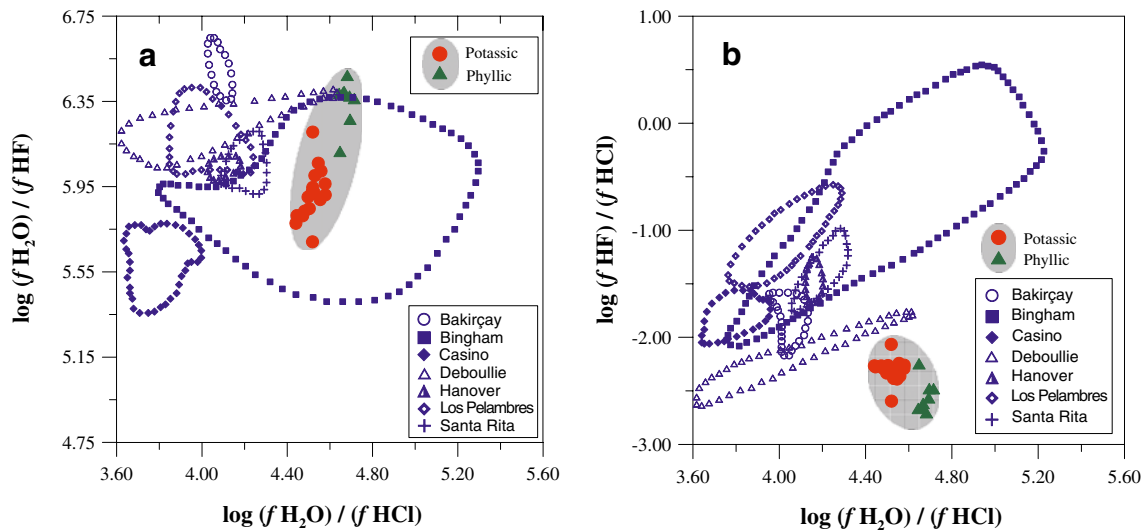


Fig. 10 Comparison of the Dalli porphyry copper deposit with other porphyry systems in terms of: a $\log(fHF)/(fHCl)$ vs. $\log(fH_2O)/(fHCl)$, b $\log(fHF)/(fHCl)$ vs. $\log(fH_2O)/(fHF)$ fugacity ratios. Analytical data are taken from Selby and Nesbitt (2000) and references there in

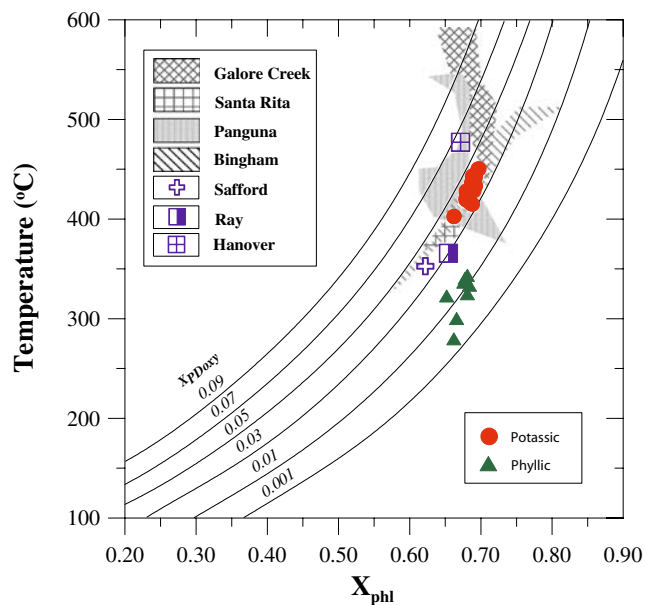


Fig. 11 Compositions of biotite from potassic and phyllic alteration zones at Dalli porphyry copper deposit on Beane's (1974) X_{phl} vs. Temperature ($^{\circ}\text{C}$) diagram. Contours show the fixed mole fractions of proton-deficient oxyannite. Analytical data for the plotting of other porphyry copper deposits including Galore Creek, Santa Rita, Safford, Ray, and Hanover are taken from Beane (1974). Single symbols represent the mean compositions of hydrothermal biotite from potassic alteration assemblages of related porphyry copper deposits. Biotite compositions from Panguna and Bingham porphyry copper deposit are taken from Ford (1978) and Laner et al. (1978), respectively

emplaced within the UMDA that extends from NW to SE in Iran and forms a zone of $2000 \times 50 \times 4$ km volcano-plutonic belt. The Dalli porphyry copper prospect area, which is located on the western boundary of UDMA, is restricted to the calc-alkaline Miocene–Pliocene subvolcanic plutons that intruded into the volcanic rocks and variety of sedimentary sequences within the UMDA. The Dalli is a moderate to small, locally Au-rich, porphyry copper deposit comprising typical porphyry style alteration zones and ore mineral assemblage. The principal opaque phases in VPR are magnetite, hematite, chalcopyrite and pyrite. The hydrothermal alteration and porphyry style Cu–Au mineralization processes at Dalli are related to the emplacement of Post-Miocene subvolcanic plutonic rocks. These processes at Dalli consist of potassic (secondary biotite–quartz–magnetite assemblage), phyllic (sericite–quartz–chlorite–specularite assemblage), propylitic (sericite–epidote–chlorite assemblage) and locally argillic zones within the subvolcanic plutons and volcanic rocks containing diorite, quartz-diorite, tonalite, granodiorite, andesite and dacite. Early hydrothermal alteration at Dalli is dominantly potassic and it seems that was subsequently followed by later phyllic, propylitic,

and locally argillic alteration processes. These distinguished alteration zones vary from a potassic core to an outer propylitic alteration zone that forms as a broad halo around the other alteration types. The Potassic alteration is characterized by the development of secondary biotite, magnetite and relict of K-feldspar within the groundmass of VPR. Amphiboles are very sensitive to potassic alteration and have been replaced by secondary biotite, sericite, and chlorite. The phyllic alteration has been quite destructive on the VPR, commonly with complete replacement of the original minerals by the secondary occurrences. Sericite and chlorite are the diagnostic phases in phyllic alteration process. This alteration is associated with numerous quartz veins including variable amount of pyrite, specularite, and chalcopyrite. The propylitic alteration is widespread in the Dalli porphyry copper deposit and has been characterized by the chloritization of biotite and other ferromagnesian minerals within the groundmass of VPR. Sericite, chlorite, calcite, and epidote are the characteristic constituents of propylitic alteration zone.

At Dalli, biotite from the potassic alteration zone is characterized by relatively high K and X_{Mg} , and low Al contents. Biotites from the phyllic zone have low Fe and Na contents. In general, biotite grains in phyllic zone are enriched in F and Cl contents, in contrast to biotite grains in potassic alteration zone. This may be interpreted as the effective overprint procedure by hydrothermal fluids of magmatic derivation those with hydrothermal fluids of meteoric origin during the hydrothermal evolution of porphyry system at Dalli. The mole fraction of phlogopite (Ph) in potassic alteration zone is higher than the phlogopite content from the phyllic zone (see Table 1). The mole fraction of titanobiotite (Tib) shows no distinctive variation for biotites in the potassic and phyllic zones, but tends to slightly increase in biotite from potassic alteration zone. The mole fraction of proton-deficient oxyannite (PDO) for biotite in the potassic alteration zone of Dalli subvolcanic plutons exhibits an enrichment trend on the contrary to biotite from the phyllic zone. Except for biotites in the phyllic zone, the Fe–F avoidance principle is consistent with biotites from the potassic alteration zone. The chemistry of biotite from the potassic zone suggests that fluids altered part of the potassic zone at a temperature range between 402° and 450°C (mean= 430°C) on the basis of biotite geothermometer proposed by Beane (1974). Application of biotite geothermometer to biotites from the phyllic alteration zone shows that hydrothermal fluids, which are responsible for biotitization temperature at Dalli ranges from 280° to 343°C (mean= 323°C). In $\log (f_{\text{HF}}/f_{\text{HCl}})$ vs. $\log (f_{\text{H}_2\text{O}}/f_{\text{HCl}})$ and $\log (f_{\text{H}_2\text{O}}/f_{\text{HF}})$ vs. $\log (f_{\text{H}_2\text{O}}/f_{\text{HCl}})$ plots, the potassic hydrothermal fluids have higher $\log (f_{\text{H}_2\text{O}}/f_{\text{HCl}})$ values than those fluids associated with the phyllic alteration zone. Fugacity ratios [$\log (f_{\text{HF}}/$

/HCl)] for biotites from the potassic zone exhibit, in general, higher values than the phyllic zone. This suggests that hydrothermal fluids associated with the potassic alteration are distinctively different from fluids related to the phyllic zone at Dalli porphyry copper deposit. The log (f_{H_2O}/f_{HCl}) ratio for hydrothermal fluids in potassic and phyllic zones at Dalli porphyry copper deposit displays typical trend with the compositional range at Bingham porphyry copper deposit. The log (f_{H_2O}/f_{HF}) ratio variation estimated for hydrothermal fluids is consistent with the log (f_{H_2O}/f_{HF}) ratio specified for Bingham, Santa Rita, Deboullie, Los Pelambres and Honover porphyry copper systems. When compared to the other porphyry copper deposits such as Bakırçay, Santa Rita, Casino, Bingham, Los Pelambres and Hanover, the log (f_{HF}/f_{HCl}) ratio for hydrothermal fluids at Dalli porphyry copper system presents a distinctive difference with less log (f_{HF}/f_{HCl}) ratio values.

Acknowledgments This study forms the part of a PhD research of senior author carried out by the adviser of *HA Haroni* at Isfahan University, Iran. The authors thank the staff of office of graduate studies at Isfahan University for their supports. We would like to express our appreciation to Dr. M. Khalili, Department of Geology, Isfahan University for his valuable suggestions. Special thanks are due to Dr. M. A. Mackizadeh for his hospitality and patient guidance at his mining company during the field studies. Saeed Mahdevari at Department of Mining, Isfahan University of Technology, is thanked for his helpful comments and continued friendship. This paper benefited from the valuable comments and suggestions of two anonymous referees. We are grateful to Dr. Anton Beran for his editorial handling.

References

- Angelkov K, Parvanov B (1980) The Assarel porphyry copper deposit, Bulgaria. In: Janković S, Sillitoe RH (eds) European copper deposits. Society of Applied Ore Deposits, Special Publication 1, pp 59–62
- Bailey SW (1980) Summary and recommendations of AIPEA Nomenclature Committee. *Clay Miner* 28:73–78
- Beane RE (1974) Biotite stability in the porphyry copper environment. *Econ Geol* 69:241–256
- Bowman JR, Parry WT, Kropp WP, Kruer SA (1987) Chemical and isotopic evolution of hydrothermal solutions at Bingham, Utah. *Econ Geol* 82:395–428
- Cathelineau M (1988) Cation site occupancy in chlorites and illites as a function of temperature. *Clay Miner* 23:471–485
- Dymek RF (1983) Titanium, aluminum and interlayer cation substitutions in biotite from high-grade gneisses, west Greenland. *Am Mineral* 68:880–899
- Emami MH (1991) Explanatory text of the Qom, Geological Quadrangle Map, 1:250,000, Geological Survey of Iran, No. E6
- Ford JH (1978) A chemical study of alteration at the Panguna porphyry copper deposit, Bougainville, Papua New Guinea. *Econ Geol* 73:703–720
- Foster MD (1960) Interpretation of the composition of trioctahedral micas. *US Geol Surv, Prof Pap* 354-B:1–146
- Gatter I, Földessy J, Zelenka T, Kiss J, Szebényi G (1999) High and low-sulfidation epithermal mineralization of the Mátra Mountains, Northeast Hungary. In: Molnár F, Lexa J, Hedenquist JW (eds) Epithermal mineralization of the western Carpathians. Society of Economic Geology Guidebook Series 31, pp 155–180
- Haroni HA (2005) Preliminary Exploration at Dalli Porphyry Cu-Prospect, Central Province of Iran, DORSA Engineering Limited, pp 22
- Hey MH (1954) A new review of the chlorites. *Mineral Mag* 30:277–292
- Hezarkhani A (2006a) Fluid inclusion investigations of the Raigan porphyry copper system, Kerman-Bam, Iran. *Int Geol Rev* 48:255–270
- Hezarkhani A (2006b) Hydrothermal evolution of the Sar-Cheshmeh porphyry Cu–Mo deposit, Iran: evidence from fluid inclusion. *J Asian Earth Sci* 28:409–422
- Hezarkhani A, Williams-Jones AE (1998) Controls of alteration and mineralization in the Sungun porphyry copper deposit, Iran: evidence from fluid inclusion and stable isotopes. *Econ Geol* 93:651–670
- Jacobs DC, Parry WT (1979) Geochemistry of biotite in the Santa Rita Porphyry copper deposit, New Mexico. *Econ Geol* 74:860–887
- Jelanković R, Vakanjac B (1999) Paragenetic features and model of development of the Veliki Krivelj copper deposit (Serbia). *Geol Macedonica* 13:23–30
- Lainer G, Raab WJ, Folsom RB, Cone S (1978) Alteration of equigranular monzonite, Bingham Mining District, Utah. *Econ Geol* 73:1270–1286
- Loferski PJ, Ayuso RA (1995) Petrography and mineral chemistry of the composite Deboullie pluton, northern Maine, USA: implications for the genesis of Cu–Mo mineralization. *Chem Geol* 123:89–105
- Melfos V, Vavelidis M, Christofides G, Seidel E (2002) Origin and evolution of the Tertiary Maronia porphyry copper–molybdenum deposit, Thrace, Greece. *Miner Deposita* 37:648–668
- Milu V, Milesi J-P, Leroy JL (2004) Rosia Poieni copper deposit, Apuseni Mountains, Romania: advanced argillic overprint of a porphyry system. *Miner Deposita* 39:173–188
- Munoz JL (1984) F–OH and Cl–OH exchange in micas with applications to hydrothermal ore deposits. In: Bailey SW (ed) *Micas. Reviews in Mineralogy*, vol. 13. Mineralogical Society of America, Washington, DC, pp 469–493
- Munoz JL (1992) Calculation of HF and HCl fugacities from biotite compositions: revised equations. *Geological Society of American Abstract Programs* 24, A221
- Parry WT, Ballantyne GH, Wilson JC (1978) Chemistry of biotite and apatite from a vesicular quartz latite porphyry plug at Bingham, Utah. *Econ Geol* 73:1308–1314
- Selby D, Nesbitt BE (2000) Chemical composition of biotite from Casino porphyry Cu–Au–Mo mineralization, Yukon, Canada: evaluation of magmatic and hydrothermal fluid chemistry. *Chem Geol* 171:77–93
- Sillitoe RH, Khan SN (1977) Geology of the Saindak porphyry copper deposit, Pakistan. *Transaction Institute of Mining and Metallurgy Section B*:86, B27–42
- Taylor RP (1983) Comparison of biotite geochemistry of Bakırçay, Turkey, and Los Pelambres, Chile, porphyry copper systems. *Inst Min Met. Sec B: App Earth Sci*, B92:B16–B22
- Tischendorf G, Gottesmann B, Förster H-J, Trumbull RB (1997) On Li-bearing micas: estimating Li from electron microprobe analyses and an improved diagram for graphical representation. *Mineral Mag* 61:809–834
- Yavuz F (1997) Igneous and hydrothermal alteration biotites from the Güzelyayla porphyry copper mineralization area, northern Turkey. In: Papunen H (ed) *Mineral deposits: research and exploration—*

- Where do they meet? Proceedings of the Fourth Biennial SGA Meeting, Turku/Finland, pp 691–694
- Yavuz F (2003a) Evaluating micas in petrologic and metallogenic aspect: I—definitions and structure of the computer program Mica⁺. *Comput Geosci* 29:1203–1213
- Yavuz F (2003b) Evaluating micas in petrologic and metallogenic aspect: Part II—Applications using the computer program Mica⁺. *Comput Geosci* 29:1215–1228
- Zarasvandi A, Liaghat S, Zentilli M (2005) Geology of the Darreh-Zerreshk and Ali-Abad porphyry copper deposits, central Iran. *Int Geol Rev* 47:620–646
- Zhu C, Sverjensky DA (1991) Partitioning of F–Cl–OH between minerals and hydrothermal fluids. *Geochim Cosmochim Acta* 55:1837–1858
- Zhu C, Sverjensky DA (1992) F–Cl–OH partitioning between biotite and apatite. *Geochim Cosmochim Acta* 56:3435–3467